

# We are IntechOpen, the world's leading publisher of Open Access books Built by scientists, for scientists

**5,600**

Open access books available

**137,000**

International authors and editors

**170M**

Downloads

Our authors are among the

**154**

Countries delivered to

**TOP 1%**

most cited scientists

**12.2%**

Contributors from top 500 universities



**WEB OF SCIENCE™**

Selection of our books indexed in the Book Citation Index  
in Web of Science™ Core Collection (BKCI)

Interested in publishing with us?  
Contact [book.department@intechopen.com](mailto:book.department@intechopen.com)

Numbers displayed above are based on latest data collected.  
For more information visit [www.intechopen.com](http://www.intechopen.com)



## Chapter

# Structure-Property Relationships in Benzofurazan Derivatives: A Combined Experimental and DFT/TD-DFT Investigation

*Hanen Raissi, Imen Chérif, Hajer Ayachi, Ayoub Haj Said, Fredj Hassen, Sahbi Ayachi and Taoufik Boubaker*

## Abstract

In this work we seek to understand and to quantify the reactivity of benzofurazan derivatives toward secondary cyclic amines, like pyrrolidine, piperidine and morpholine, acting as nucleophile groups in  $S_NAr$  reactions. For this aim, physico-chemical and structural descriptors were determined experimentally and theoretically using the DFT/B3LYP/6-31+g(d,p) methodology. Thus, different 4-X-7-nitrobenzofurazans (X = OCH<sub>3</sub>, OC<sub>6</sub>H<sub>5</sub> and Cl) and products corresponding to the electrophilic aromatic substitution by pyrrolidine, piperidine and morpholine, were investigated. Particularly, the HOMO and LUMO energy levels of the studied compounds, determined by Cyclic Voltammetry (CV) and DFT calculations, were used to evaluate the electrophilicity index ( $\omega$ ). The latter was exploited, according to Parr's approach, to develop a relationship which rationalizes the kinetic data previously reported for the reactions of the 4-X-7-nitrobenzofurazans with nucleophiles cited above. Moreover, the Parr's electrophilicity index ( $\omega$ ) of these benzofurazans determined in this work were combined with their electrophilicity parameters (E), reported in preceding papers, was found to predict the unknown electrophilicity parameters E of 4-piperidino, 4-morpholino and 4-pyrrolidino-7-nitrobenzofurazan. In addition, the relationship between the Parr's electrophilicity index ( $\omega$ ) and Hammett constants  $\sigma$ , has been used as a good model to predict the electronic effect of the nucleophile groups. Finally, we will subsequently compare the electrophilicity index ( $\omega$ ) and the electrophilicity parameters (E) of these series of 7-X-4-nitrobenzofurazans with the calculated dipole moment ( $\mu$ ) in order to elucidate general relationships between E,  $\omega$  and  $\mu$ .

**Keywords:** Benzofurazan, Structure–property correlations, Optical properties, Mayr's approach, Electrophilicity, Parr's approach, Voltammetry Cyclic, DFT, ICT, NLO properties

## 1. Introduction

4-Nitrobenzofurazan (NBD) is neutral  $10\pi$  electron-deficient heteroaromatic substrates. Organic materials containing the NBD moiety have been tested in

potential biomedical and bio-analytical applications. [1–7] They have been also used as an effective electron-withdrawing building block for organic solar cell materials [8], and have been discovered to be nonlinear optical (NLO) materials. [9] In addition, the strong electron withdrawing properties of nitrobenzofurazan (NBD) derivatives make it an exceptional electrophilic product of the nucleophilic aromatic substitution ( $S_NAr$ ).

In addition, the activated chlorine atom in 4-chloro-7-nitrobenzofurazan (NBD chloride, namely NBD-Cl) can undergo electrophilic aromatic substitution by phenoxide, primary or secondary cyclic amines [10–13] and some of 4,7 di-substituted benzofurazan compounds to generate weakly or non-fluorescents products. [14–18]

A previous kinetic study of amino-substituted NBD showed that methoxy and aryloxy substituent's are better leaving groups than chloro and that a red-colored Meisenheimer complex immediate was formed during the reactions [19].

On the other hand, the frontier molecular orbital descriptors including HOMO and LUMO energy levels play major roles in governing many chemical reactions as function of reactivity and stability of related molecules. [20, 21] Alternatively, contacts from intra-molecular interactions have been identified as an important driving force on the stabilization of various planar molecular structures. [22, 23] However, these interactions lead to intra-molecular charge transfer of formed compounds and thus provides a non-radiative decay from the excited state. [24–26]

Recently, we reported a kinetic study for  $S_NAr$  reactions of NBD with secondary amines. [27–30] The present chapter is focused on the elucidation of the combined experimental–theoretical investigation relationships between the optical (UV–Vis, PL and time resolved photoluminescence (TR-PL), electrochemical (CV) properties and the chemical structures of 4,7-di-substituted benzofurazans (NBDs), based on the kinetic reactivity process of compounds. Parr's approach was employed to develop a relationship which rationalizes the kinetic data previously reported for the reactions of 4-X-7-nitrobenzofurazans with various nucleophiles. [27–29].

Then, the substituent effects were particularly limited only to morpholine, piperidine and pyrrolidine groups. Thus, we seek to study the structure–property relationships for molecules containing 4-nitrobenzofurazan moiety for a better understanding of their optical behavior and their chemical reactivity. For this aim, theoretical calculations using quantum chemical calculations within density functional theory (DFT) and its extension TD-DFT in the 6-31 + g(d,p) basis set have been developed to facilitate the in-depth understanding of structure–property relationships.

The Molecular structures of the investigated compounds are illustrated in **Figures 1** and **2**.

To the best of our knowledge, no similar study has been published on electrochemical and photo-physical properties of the studied compounds. Cyclic Voltammetry (CV) is used to estimate the band gaps, electron affinities (i.e. the

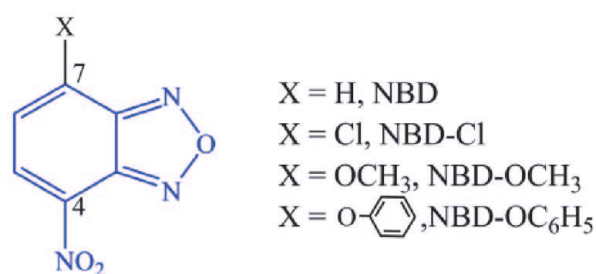


**Figure 1.**  
Chemical structures of the studied electrophile compounds.

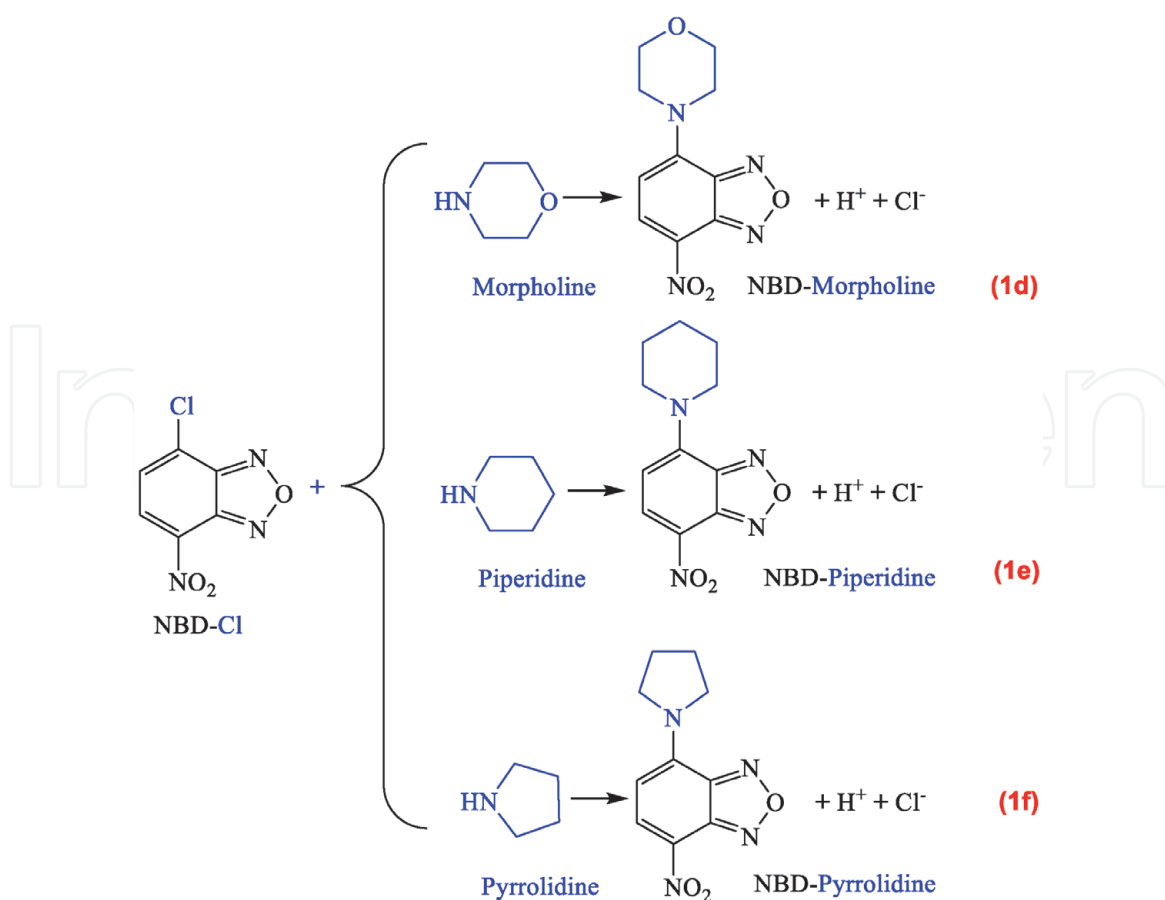


**Figure 2.**  
Reaction mechanism between NBD-Cl and three examples of nucleophiles (morpholine, piperidine and pyrrolidine) groups.

energy of LUMO,  $\epsilon_{\text{LUMO}}$ ) and ionization potentials (i.e., the energy of HOMO,  $\epsilon_{\text{HOMO}}$ ). [31] Besides, the computed results from DFT and TD-DFT calculations enable the access to the structure geometry, the Mullikan charge distribution and the dipole moment of the 4,7 di-substituted benzofurazan at the ground- ( $S_0$ ) and excited ( $S_1$ )-states. [32, 33]

## 2. Experimental details

### 2.1 Materials

The 7-chloro-4-nitrobenzofurazan (NBD-Cl) and the tetraethyl ammonium tetrafluoroborate (TEAF) were commercial products (Aldrich, Darmstadt-Germany). Samples of 7-methoxy-4-nitrobenzofurazan (NBD-OCH<sub>3</sub>) and 7-phenoxy-4-nitrobenzofurazan (NBD-OC<sub>6</sub>H<sub>5</sub>) were prepared according to the standard methods described in the literature. [27–29] The secondary cyclic amines (morpholine, piperidine and pyrrolidine) were commercial products (Aldrich, Darmstadt-Germany) and were redistilled before use whenever necessary.

### 2.2 Apparatus

Cyclic Voltammetry (CV) measurements were carried out under nitrogen gas with a Voltalab 10 apparatus from Radiometer driven by the Volta Master software at a potential scan rate of 0.1 V/s, at room temperature, in 25 mL of CH<sub>3</sub>CN solution

containing TEAF (0.1 M) as a supporting electrolyte. The cell used three electrodes. The working electrode was a 2 mm diameter platinum disk (Tacussel type EDI) and a platinum (Pt) wire as a counter electrode. The concentrations of the substrates were  $10^{-3}$  M. The potentials  $E_{\text{Ox}}$  and  $E_{\text{Red}}$  give us the information on HOMO and LUMO energy levels of studied materials.

The UV-visible absorption spectra of compounds have carried out on a Shimadzu UV-visible model 1650 spectrometer. The samples were dissolved in acetonitrile medium. The optical properties of the sample are secondly investigated by photoluminescence spectroscopy. The 514.5 nm line of the continuous-wave argon Ar + laser is used as an excitation source. Spectral analysis of the PL was performed using a Jobin Yvon iHR320 monochromator through the lock-in amplifier technique.

For the Time-Resolved PL (TRPL) study, the sample was illuminated by a pulsed laser diode with photon energy of 1.58 eV with a repetition rate of 80 MHz, using the time correlated photo counting technique. The details experiment was reported elsewhere. [34]

## 2.3 Computational methods

Ground-state ( $S_0$ ) optimized geometries of the studied compounds were performed by means of DFT at B3LYP level of theory [35, 36] in conjunction with the 6-31+ g(d,p) basis set. No constraints were used and all structures were free to optimize in an acetonitrile solution by applying the conductor polarizable continuum model (CPCM) with the Gaussian 09 program [37] and the output files were visualized with the Gauss View (5.0.8) molecular visualization program. [38] To predict the optical absorption properties of the studied compounds, UV-Vis absorption spectra were simulated at the time-dependent TD-DFT level with the same basis set. The electronic properties such as highest occupied molecular orbital ( $\epsilon_{\text{HOMO}}$ ) and lowest unoccupied molecular orbital ( $\epsilon_{\text{LUMO}}$ ) energy levels and dipole moment have been extracted from calculations.

The semi-empirical quantum-chemical ZINDO level was used to predict the optical emission spectra on  $S_1$  optimized structures. Electronic transitions assignment and oscillator strengths were also calculated using the same method of calculations.

## 3. Results and discussion

### 3.1 Electrochemical analysis

Electrochemical comparative studies were undertaken using Cyclic Voltammetry (CV) for the six compounds 4,7 di-substituted benzofurazan (See **Figures 3** and **4**). The CVs profiles were performed in the potential range of  $-2.0$  to  $+3.0$  V.

The potentials ( $E_{\text{OX}}$  and  $E_{\text{Red}}$ ) peaks can be used to determine the HOMO and LUMO energy levels of the studied compounds. Indeed, the value of their energy gaps can be estimated from the potentials difference.

The highest occupied molecular orbital (HOMO) energy and the lowest unoccupied molecular orbital (LUMO) energy were estimated from the first oxidation and reduction potentials, respectively. The energy levels were calculated according to an empirical method [39] and by assuming that the energy level of the ferrocene/ferrocenium is 4.8 V below the vacuum level.



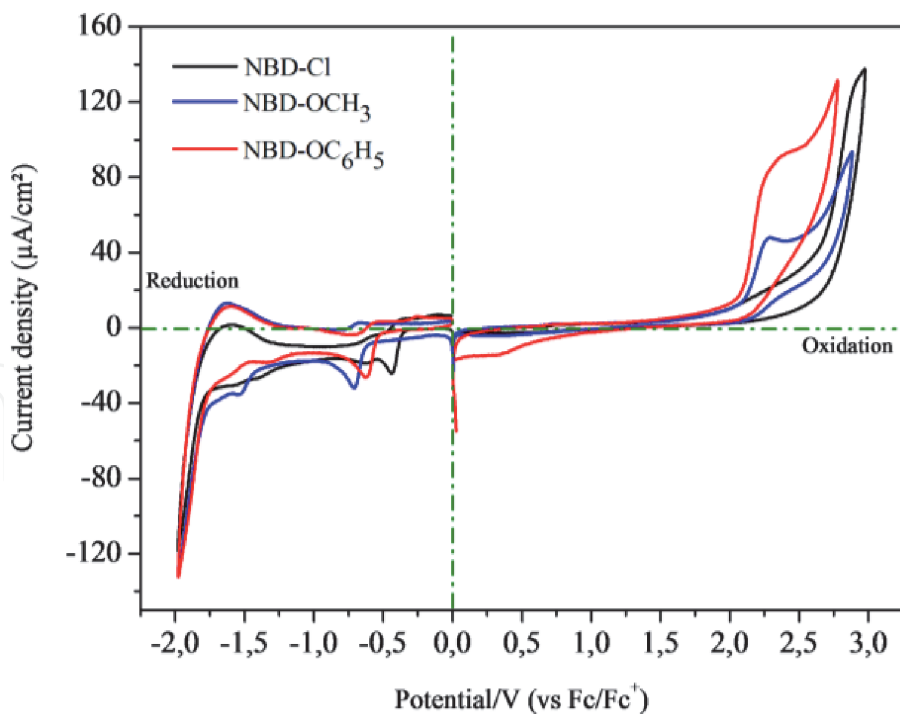


**Figure 3.**  
 Oxidation and reduction voltammograms of NBD-Cl, NBD-OCH<sub>3</sub> and NBD-OC<sub>6</sub>H<sub>5</sub> products (10<sup>-3</sup> M) recorded in acetonitrile.

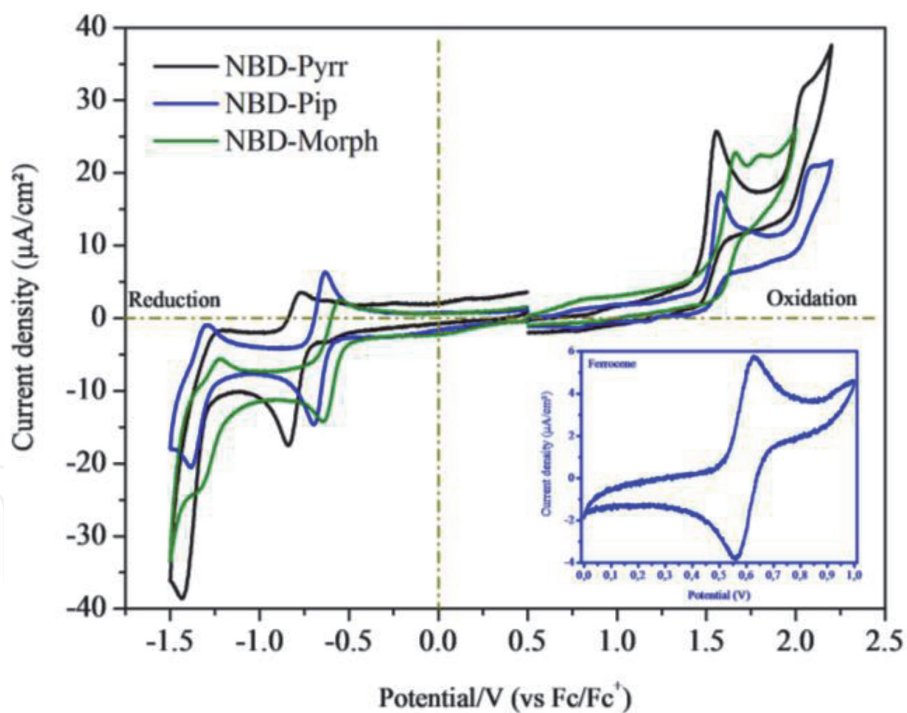


**Figure 4.**  
 Oxidation and reduction voltammograms of NBD-Pyrr, NBD-pip and NBD-Morph products (10<sup>-3</sup> M) recorded in acetonitrile.

$$\epsilon_{\text{HOMO}} = -e \left[ E_{\text{OX}} - E_{\text{Fc/Fc}^+}^0 \right] - 4.8 \quad (1)$$

$$\epsilon_{\text{LUMO}} = -e \left[ E_{\text{Red}} - E_{\text{Fc/Fc}^+}^0 \right] - 4.8 \quad (2)$$

Here,  $E_{\text{Ox}}$  and  $E_{\text{Red}}$  are the potential of the oxidation peak and reduction peak, respectively. These values were obtained from the CV curve for each compound;

$E_{\text{Fc}/\text{Fc}^+}^0$  is 0.59 eV, the average of oxidation and reduction peak potentials of ferrocene measured under the same experimental condition; 4.8 eV is the energy difference between the energy level of ferrocene and the vacuum. Note that when the oxidation/reduction peak of the studied compound was reversible, the  $E_{\text{ox/red}}$  was replaced in the equation by  $E^{\circ}_{\text{ox/red}}$  determined experimentally.

For the electrophile compounds (**Figure 3** and **Table 1**), the peaks appeared at the reduction potentials of about: -0.440 V (NBD-Cl), -0.716 (NBD-OCH<sub>3</sub>) and -0.610 V (NBD-OC<sub>6</sub>H<sub>5</sub>). They correspond to LUMO energy levels at -3.77 eV, -3.49 eV and -3.60 eV, respectively. In the same way, the oxidation potentials located at: 2.90 V, 2.28 V and 2.40 V led to HOMO energy level values of -7.11 eV, -6.49 eV and -6.61 eV for NBD-Cl, NBD-OCH<sub>3</sub> and NBD-OC<sub>6</sub>H<sub>5</sub>, respectively. The electrochemical energy gaps deduced from these measurements were: 3.34 eV (NBD-Cl), 3.00 eV (NBD-OCH<sub>3</sub>) and 3.01 eV (NBD-OC<sub>6</sub>H<sub>5</sub>).

For the three first compounds used as electrophile groups, they were oxidized and reduced at relatively distinct potentials. Indeed, the NBD-Cl is oxidized and reduced at higher potentials than methoxy and phenoxy substituted NBD.

For the amino-substituted NBD (**Figure 4** and **Table 1**), the oxidation potential peak values were detected nearly 1.66 V, 1.58 V and 1.55 V for morpholine, piperidine and pyrrolidine substituted NBD, respectively. They correspond to HOMO energy levels at -5.87 eV, -5.79 eV and -5.76 eV, respectively. However, the reduction peaks of the studied compounds were reversible and thus the  $E_{\text{Red}}$  was replaced in the equation by  $E_{\text{Red}}^0$  determined experimentally. Accordingly, the estimated LUMO energy levels are of about: -3.62 eV (NBD-Morph), -3.55 eV (NBD-Pip) and -3.41 eV (NBD-Pyrr).

Compounds	Cyclic voltammetry (CV)							
	$E_{\text{Ox}}$ (V vs. FC/FC <sup>+</sup> )	$E_{\text{Red}}$ (V vs. FC/FC <sup>+</sup> )	$E_{\text{Red}}^0$ (V)	Energy levels		Chemical reactivity descriptors		
				$\epsilon_{\text{HOMO}}^{\text{CV}}$ (eV)	$\epsilon_{\text{LUMO}}^{\text{CV}}$ (eV)	$\mu$ (eV)	$\eta$ (eV)	$W^{\text{CV}}$ (eV)
NBD-Cl	2.90	-0.44	—	-7.11	-3.77	-5.44	1.67	8.86
NBD-OCH <sub>3</sub>	2.28	-0.71	—	-6.49	-3.49	-4.99	1.50	8.30
NBD-OC <sub>6</sub> H <sub>5</sub>	2.40	-0.61	—	-6.61	-3.60	-5.10	1.51	8.65
NBD-Morph	1.66	-0.64	-0.59	-5.87	-3.62	-4.74	1.13	9.94
NBD-Pip	1.58	-0.70	-0.66	-5.79	-3.55	-4.66	1.12	9.67
NBD-Pyrr	1.55	-0.84	-0.80	-5.76	-3.41	-4.58	1.18	8.88

**Table 1.** Calculated HOMO and LUMO energy levels and extracted chemical reactivity descriptors for studied compounds.

## 3.2 Photo-physical properties

### 3.2.1 UV-Vis optical absorption and emission (PL) analysis

The optical absorption spectra of the four substituted benzofurazans (NBDs) compounds are illustrated in **Figure 5**. The NBD-Cl, as starting material, has two distinct absorption bands (262 nm and 337 nm). The spectral characteristics of NBD-Cl were maintained and appeared as the same general features for

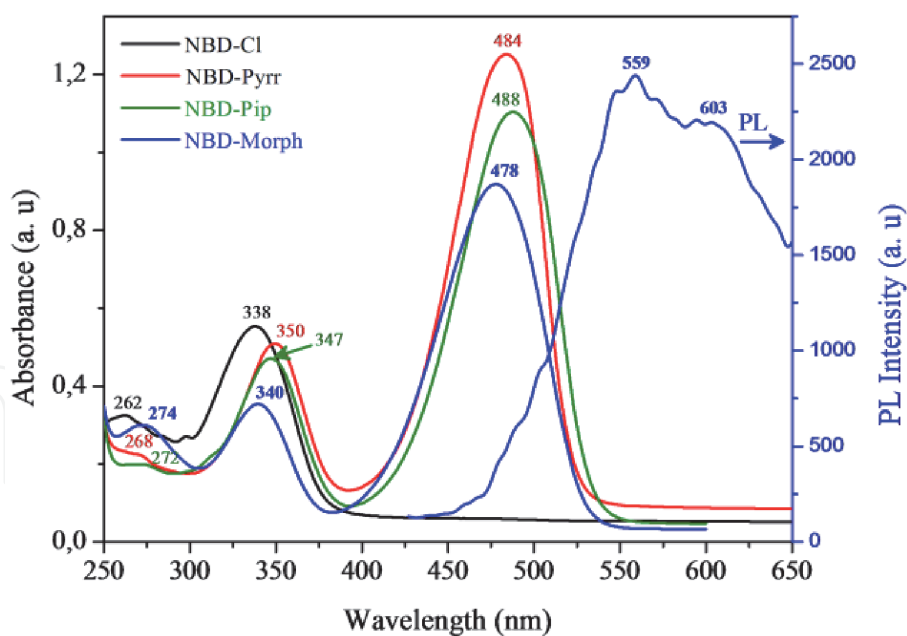


**Figure 5.**  
*Experimental UV-vis optical absorption spectra of studied compounds as well as experimental PL spectrum of NBD-Morph.*

amino-NBD derivatives. For the later systems, a new optical band in the range 478-488 nm was assigned to the formation of amino-NBD derivatives by  $S_NAr$  reactions. In fact, typical three distinct absorption bands are presented for NBD substituted with pyrrolidine, piperidine or morpholine, similar to that previously reported NBD-amino derivatives [1-3]. Besides, the maximum absorption wavelengths of amino-NBD derivatives shifted more bathochromically than that of NBD-Cl.

According to assignments reported previously by Heberer and coworkers for NBD-amino derivatives [40] the short-wavelength band is associated to the aromatic benzofurazan compounds. The middle band at around 340 nm was attributed to a  $\pi \rightarrow \pi^*$  electronic transition. However, the band with lower energy in the range of 478-487 nm has ascribed to ICT arranged between the electron-donor and the nitro ( $NO_2$ ) electron-withdrawing groups within the molecule) (NBD-Cl, free band). Importantly, the maxima for the charge transfer band in these systems are detected in the visible region of the spectra.

In addition, similar profiles of optical absorption spectra for amino-NBD were obtained. Thus, the excitation corresponding to the lowest energy band of title compounds was used in order to investigate the excitation process from the ground ( $S_0$ ) to the first excited state ( $S_1$ ).

Experimentally, the 4,7-disubstitued benzofurazan compound, NBD-Morph was excited at the maximum absorption wavelength and show two distinct fluorescence bands (See **Figure 5**). The PL spectrum shows of two dominant features peaking at approximately 2.21 eV (559 nm) and 2.05 eV (603 nm), thus, a broad green to orange emission band has been identified for the tested NBD-Morph compound.

### 3.2.2 Time-resolved photoluminescence (TR-PL) decay kinetics

The performed time-resolved photoluminescence (TR-PL) decay kinetics is analyzed and illustrated by experiment (**Figure 6**). A particular attention is devoted to the thorough analysis of non-exponential decay kinetics. However, the TR-PL decay recorded at longer wavelength emission was relatively affected. It should be mentioned that lifetimes are inaccessible from the decay process by the use



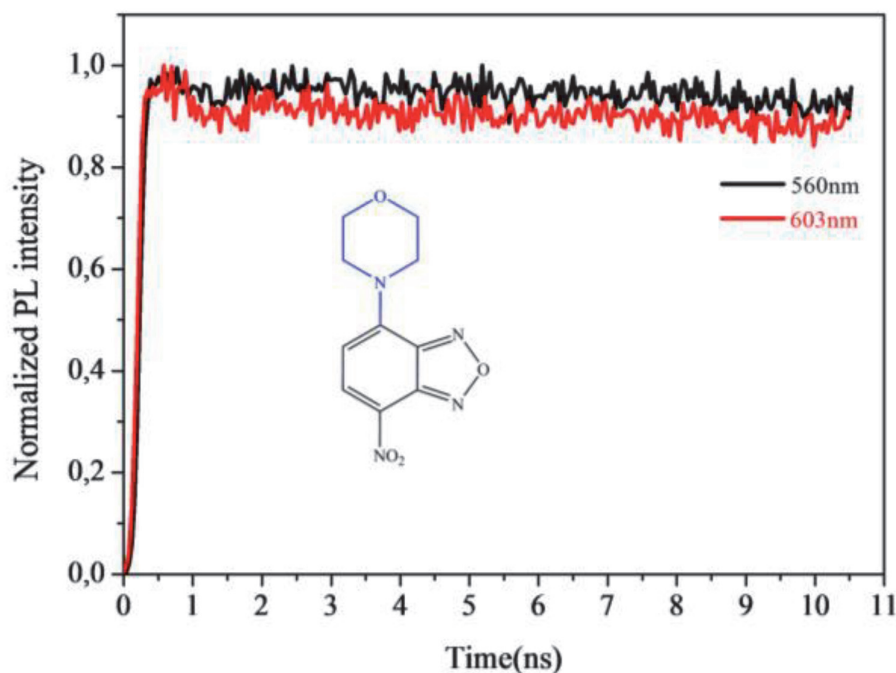


**Figure 6.**  
Time-resolved decay curves recorded at emission energy of 2.21 eV (560 nm) and 2.05 eV (603 nm) for NBD-Morph film.

experimental equipment and could be related to an efficient intra-molecular charge transfer occurred in NBD-Morph molecule. The result was supported by the ICT characteristic optical band for a compound that had a lower intensity compared to those of analogue compounds (See **Figure 5**). The flat TR-PL spectrum means that the photo-carriers have a long lifetime (more than the nanosecond regime), leading to an important diffusion length.

### 3.3 Quantum chemistry computation results

Complete geometry optimizations of studied compounds were firstly carried out at DFT using B3LYP functional and the polarized 6-31 g+(d,p) basis set. The optimized molecular structures are illustrated in **Figure 7**. Particularly, the title amino-NBD compounds contain mainly three types of chemical bonds, namely O—H, N—H and N—O which are associated to an intra-molecular non covalent interactions.

The computed geometrical parameters related to the short contacts at ground ( $S_0$ ) and excited ( $S_1$ ) states are given in **Figure 7** and tabulated in **Table 2**. The  $S_0$  calculated short contact O—H was 2.39 Å (versus 2.38 Å,  $S_1$ ) in all systems,

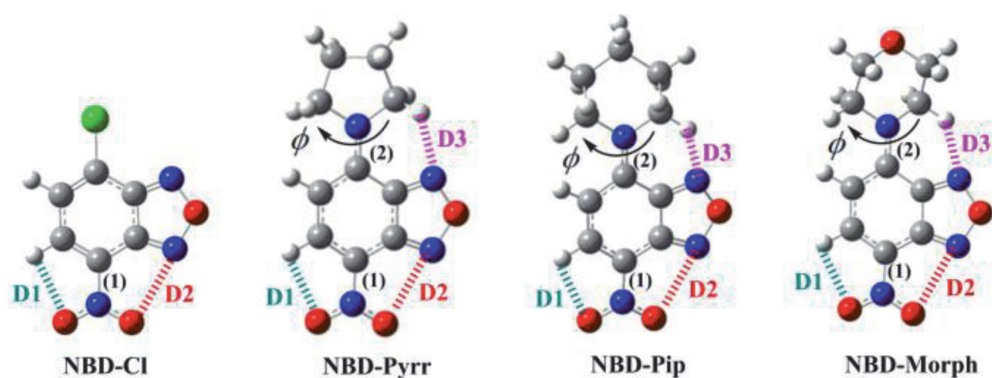


**Figure 7.**  
Molecular optimized structures with intra-molecular short contacts.

	Intra-molecular Short Contacts			Covalent contacts		Dihedral Angle	Dipole Moment (D)
	D1 O—H (Å)	D2 N—O (Å)	D3 N—H (Å)	dC-N (1) (Å)	dC-N (2) (Å)	$\phi$ (°)	
NBD-Pyrr	2.39 (2.38)	2.78 (2.74)	2.47 (2.53)	1.41 (1.37)	1.33 (1.32)	3.47 (5.75)	17.08 (17.45)
NBD-Pip	2.39 (2.38)	2.78 (2.74)	2.11 (2.25)	1.41 (1.37)	1.34 (1.33)	9.66 (16.76)	16.84 (16.53)
NBD-Morph	2.39 (2.38)	2.78 (2.74)	2.11 (2.22)	1.41 (1.37)	1.35 (1.33)	5.16 (12.34)	13.57 (13.95)

**Table 2.** Calculated non covalent interactions for O—H N—O and N—H participating in short intra-molecular contacts within molecular at ground ( $S_0$ ) and excited ( $S_1$ ) states. The values presented in parentheses are obtained at  $S_1$ .

considerably smaller than the sum of the van der Waals radii (2.72 Å). The N—O short contact is found 2.78 Å versus 2.74 Å,  $S_1$ ) significantly too smaller than the sum of the van der Waals radii (3.07 Å). In addition, the third short contact of N—H (smaller than the sum of the van der Waals radii (2.75 Å)) is allowed to vary from 2.11 Å -2.47 Å ( $S_0$ ) to 2.22 Å-2.53 Å ( $S_1$ ). The later (N—H) contacts are sensitive to amino substituted groups. As a result, these contacts have been identified as an important driving force on the stabilization of the studied co-planar molecular structures. [41] The major difference in the ground and excited state is the change in torsional angle  $\phi$  and in the dipole moment. Calculations reveal that the existence of the amino groups significantly modifies the properties of their excited states. While the ground state is predicted to be planar, the excited-state geometry is twisted by about 2-7°. Due to conformational changes, the singlet excited-state dipole moment was found to be greater than ground-state dipole moment, unexpected for NBD-Pip (16.84 D ( $S_1$ ) versus 16.53 D ( $S_0$ )). Importantly, the C-NO<sub>2</sub> bond lengths indexed as (1) decreases by 0.4 Å upon excitation, due the nitro strong electron-withdrawing group effect.

Note that the band gap values estimated using the electrochemical method may be different from those calculated by optical or theoretical methods (see **Table 3**). This result could be explained by the fact that the oxidation/reduction process at the electrode are reactions generating species in ground states, whereas the optical electron transition leads to the formation of excited states. Moreover, the electro-generation of a radical cation or radical anion in solution involves other thermodynamic (salvation ...) and kinetic effects. Consequently, it is expected that the peak

Compounds	Energy levels		Chemical reactivity descriptors			IP(eV)	EA(eV)
	$\epsilon_{\text{HOMO}}$ (eV)	$\epsilon_{\text{LUMO}}$ (eV)	$\mu$ (eV)	$\eta$ (eV)	W (eV)		
X = Cl	-7.648	-3.929	-5.788	1.859	9.009	7.481	4.195
X = OCH <sub>3</sub>	-6.988	-3.561	-5.274	1.713	8.117	6.806	3.830
X = OC <sub>6</sub> H <sub>5</sub>	-6.985	-3.684	-5.334	1.650	8.620	6.629	4.041
NBD-MORPH	-6.349	-3.296	-4.822	1.526	7.617	6.081	3.672
NBD-Pip	-6.238	-3.190	-4.714	1.524	7.290	6.013	3.607
NBD-Pyrr	-6.262	-3.151	-4.706	1.555	7.120	6.044	3.420

**Table 3.** Calculated HOMO and LUMO energy levels and extracted chemical reactivity descriptors for studied compounds using DFT//B<sub>3</sub>LYP/6-31+g(d,p) in acetonitrile.

potential will be lowered due to fast chemical reactions following the primarily electron transfer generating chemically reactive radical ions.

To better understand the optical responses, we used the time-dependent density functional theory (TD-DFT) to simulate the optical absorption spectra (See **Figure 8**). Their corresponding electronic transition assignments are given in **Table 4**. The maximum absorption wavelengths and the molecular extinction coefficients ( $\epsilon$ ) of the chloro- and amino-substituted NBD, in acetonitrile, are also given.

It is worthwhile mentioning that the extensive DFT and TD-DFT calculations show a good correlation between observed absorption and theoretical vertical excitation.

For the emission properties, it should be noted that the ZINDO semi-empirical quantum chemistry [42] was used to predict the emission spectra (See **Figure 9**). **Table 4** lists the emission optical bands of the amino substituted benzofurazan and their assignments. The emission properties are mainly from LUMO and LUMO+1 to HOMO.

It is found that compounds emit at appreciably higher wavelengths in the range 620-640 nm. It should be noted also that bathochromic effect is due to the NBD moiety and the amino substituted groups. It should be noted that NBD-Morph present absorption at wavelength maximum of 478 nm and emit orange light at 559-603 nm. This provides a large apparent Stokes shift of 81 nm attributed to the ICT process (**Table 5**). The combined experimental and computed results suggest that the new NBD-Morph compound is still considered fluorescent. Then, considerable efforts have been undertaken to test the other analogue compounds.

4-amino substituted NBD is recognized among to the broad family of intramolecular charge transfer (ICT) complexes. The ICT characteristics are identified by the presence of both electron donor and withdrawing acceptor substituent moieties within the same molecule. Thus, the photo-initiated electron transfer from the donor to the acceptor sites yields two kinds positive and negative charges within separated functional parts of the molecule. Herein, we have extracted the atomic

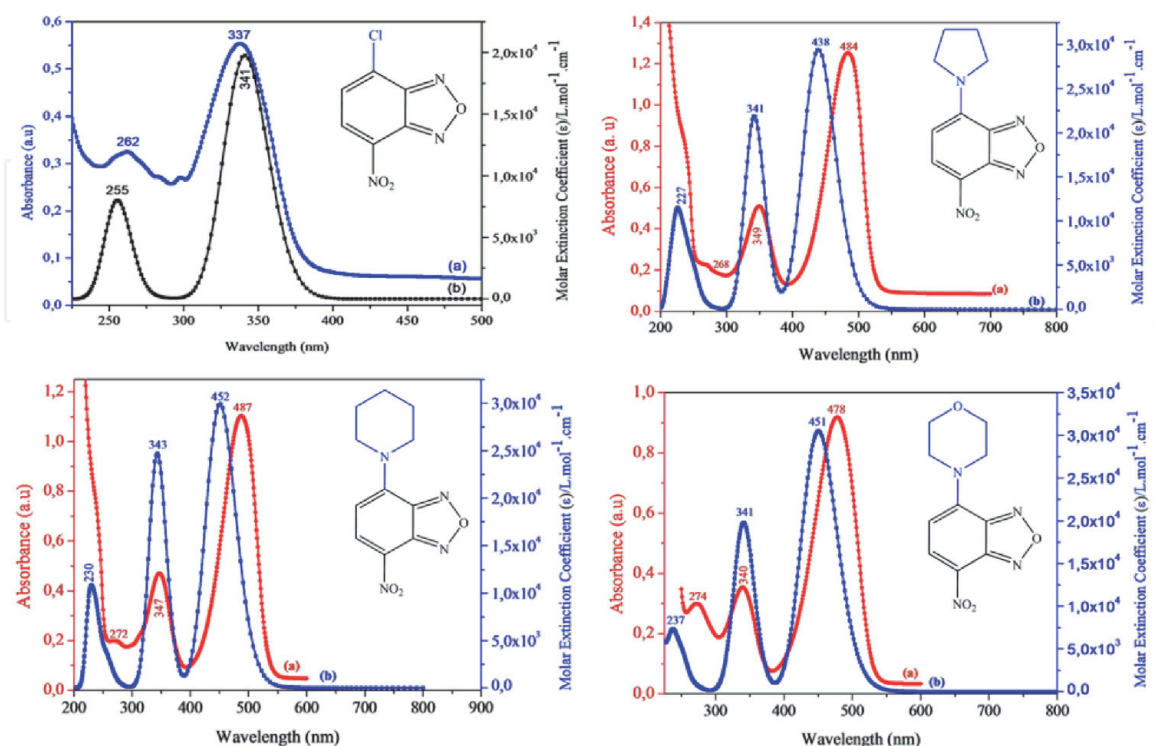


**Figure 8.**

Simulated optical absorption spectra of Cl-NBD and its related amino-substituted NBD by means of DFT//B<sub>3</sub>LYP/6-31+g(d,p) level of theory, in acetonitrile.

Compounds	$\lambda_{\max}^{\text{abs}}$ (nm)	Osc. strength	Major contribs	Minor contribs
NBD-Cl	341	0.2729	H → L (99%)	—
	255	0.0709	H-4 → L (79%)	H → L + 2 (10%) H → L + 1 (6%)
	$\lambda_{\max}^{\text{Exp}}$ : 262 nm, 337 nm			
NBD-Pyrr	227	0.0181	H → L + 3 (94%)	H → L + 5 (3%)
	341	0.2781	H → L + 1 (87%)	H-1 → L (6%) H → L (5%)
	438	0.4065	H → L (94%)	H → L + 1 (5%)
$\lambda_{\max}^{\text{Exp}}$ : 268 nm, 349 nm, 484 nm				
NBD-Pip	230	0.0012	H-7 → L (78%) H-4 → L + 1 (13%)	H-9 → L (3%) H-4 → L (2%)
	343	0.2083	H-1 → L (30%) H1 → L + 1 (59%)	H-1 → L + 1 (7%) H → L (2%)
	452	0.4129	H → L (94%)	H → L + 1 (5%)
$\lambda_{\max}^{\text{Exp}}$ : 272 nm, 347 nm, 487 nm				
NBD-Morph	237	0.0859	H → L + 2 (64%) H-3 → L + 1 (15%) H-6 → L (12%)	H-6 → L + 1 (2%)
	341	0.2608	H → L + 1 (89%)	H-1 → L (5%) H → L (4%)
	451	0.4209	H → L (95%)	H → L + 1 (4%)
$\lambda_{\max}^{\text{Exp}}$ : 274 nm, 340 nm, 478 nm				

**Table 4.** The vertical excited energies (nm) and their oscillator strengths (*f*) for the ground ( $S_0 \rightarrow S_1$ ) states of studied compounds by TD//B3LYP/6-31+g(d,p) level of theory.

Mulliken charges from both ground- and excited-geometry structures. The results are illustrated in **Figure 10**. In fact the 4-amino substituted NBD belongs to the broad family of ICT molecules, with the amino group acting as an electron donor upon photo-excitation, and the nitro ( $\text{NO}_2$ ) group as an electron acceptor.

As illustrated in **Figure 11**, we have presented the frontier molecular orbitals (FMOs) to obtain insight into the molecular structure and optoelectronic changes from the ground ( $S_0$ ) to excited ( $S_1$ ) States. We can observe that for all systems, the nitro and the 4-amino substituent groups significantly contribute to the optoelectronic properties. Particularly, the NBD-Morph differs from the other two compounds, where the oxygen atom did not contribute exclusively in excited state. This could explain the electron transfer from the nitrogen group of the electron donor moiety.

### 3.4 Relationships of chemical structure and reactivity properties

It is relevant to note that good accuracy of computational predictions of optical properties is already attainable. Accordingly, we utilize this approach for accurate prediction of the global reactivity descriptors including chemical potential ( $\mu$ ), Chemical hardness ( $\eta$ ) and electrophilicity index ( $\omega$ ) (see **Table 5**).

Parr's electrophilicity  $\omega$  values are calculated according to Eq. (3) [43, 44] based on  $\mu$  and  $\eta$  which can be evaluated using Eqs. (4) and (5).



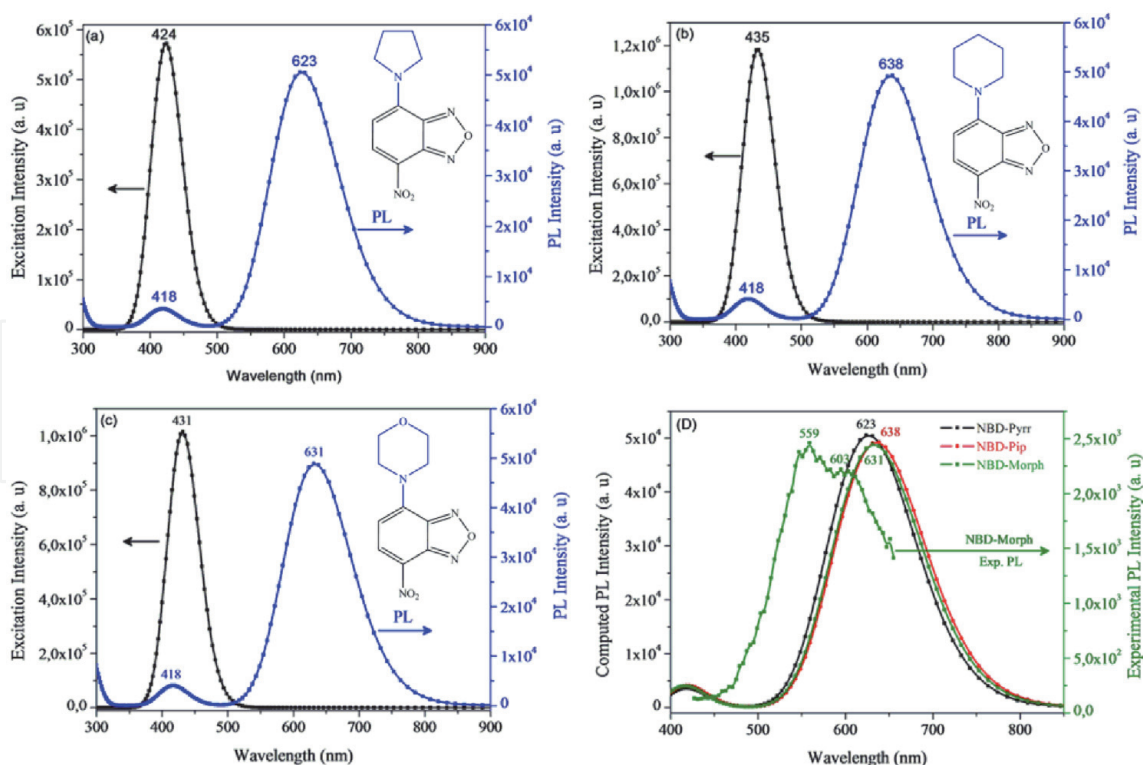


**Figure 9.** Simulated emission spectra of amino-substituted NBD compounds (a,b,c). Superposition of emission spectra with experimental data for NBD-Morph is given (Figure 9D).

Compounds	$\lambda_{\text{max}}^{\text{Em}}$ (nm)	Osc. strength	Major contribs	Minor contribs
NBD-Pyrr	418	0.0498	L + 1 $\rightarrow$ H (95%)	—
	623	0.6989	L $\rightarrow$ H (97%)	—
NBD-Pip	418	0.0564	L + 1 $\rightarrow$ H (95%)	—
	638	0.6806	L $\rightarrow$ H (97%)	—
NBD-Morph	418	0.0552	L + 1 $\rightarrow$ H (95%)	—
	631	0.6747	L $\rightarrow$ H (97%)	—

$\lambda_{\text{max}}^{\text{Exp}}$ : 559 nm, 603 nm

**Table 5.** The vertical excited energies (nm) and their oscillator strengths (f) for the  $S_1 \rightarrow S_0$  states of studied compounds obtained by ZINDO method. The wavelengths excitation was ranging from 424 to 435 nm.

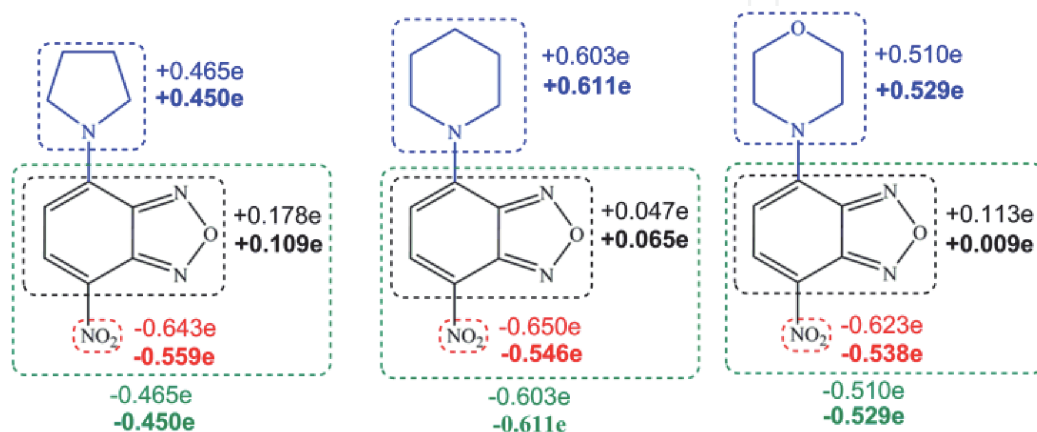


**Figure 10.** Mulliken charge distribution of ground- and excited (bold values) states optimized structures of studied compounds.



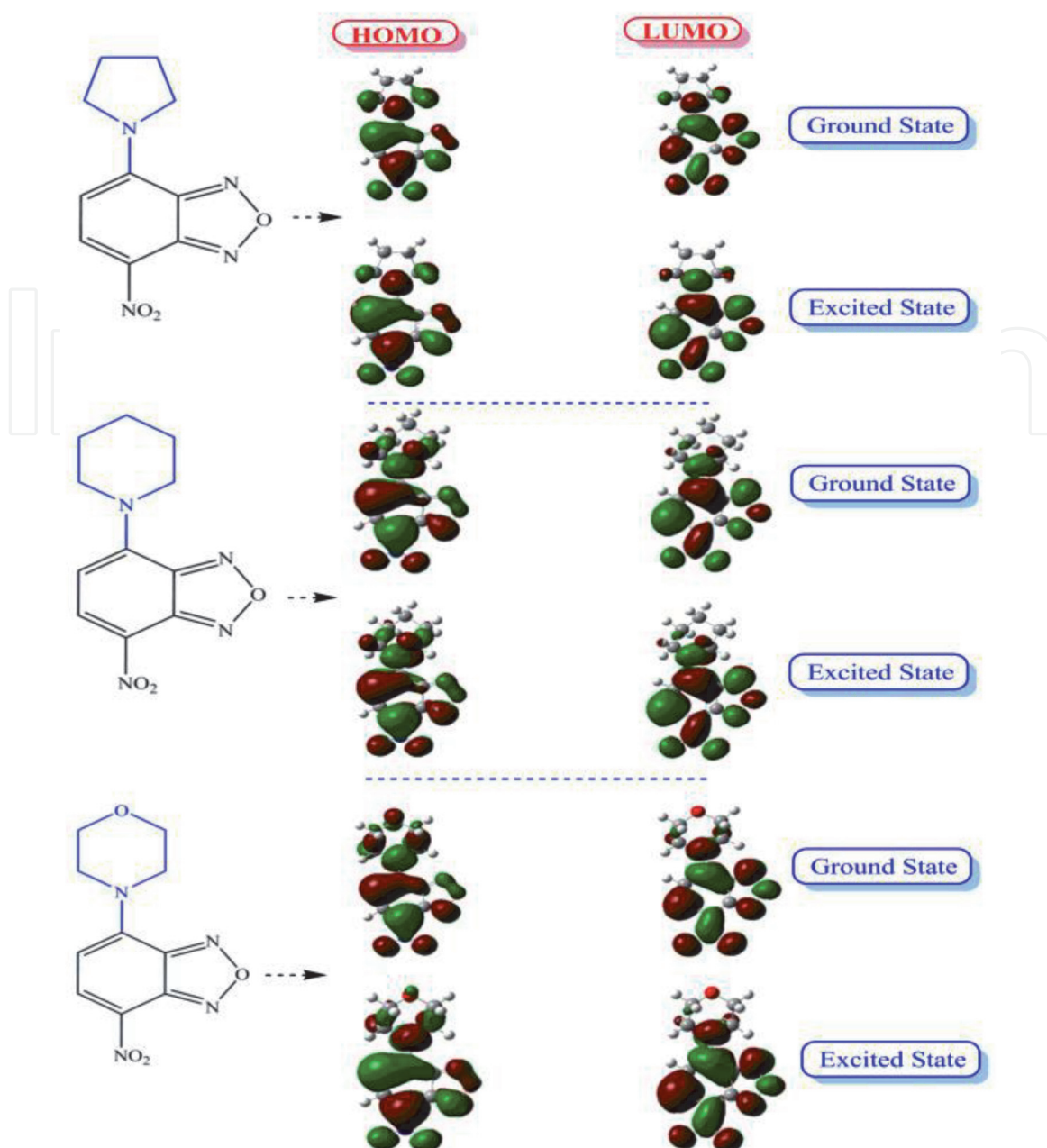


**Figure 11.** Frontier molecular orbitals (FMOS) obtained at the ground- ( $S_0$ ) and excited- ( $S_1$ ) states of the optimized geometries of studied compounds.

$$w = \frac{\mu^2}{2\eta} \quad (3)$$

$$\mu \approx \frac{1}{2}(\epsilon_{HOMO} + \epsilon_{LUMO}) \quad (4)$$

$$\eta \approx \frac{1}{2}(\epsilon_{LUMO} - \epsilon_{HOMO}) \quad (5)$$

### 3.4.1 Correlation analysis

In a recent study, we showed that the second-order rate constants for the reactions of 7-X-4-nitrobenzofurazans **1** (**1a**, X = Cl, **1b**, X = OC<sub>6</sub>H<sub>5</sub> and **1c**: X = OCH<sub>3</sub>) with secondary cyclic amines **2** (**2a**, morpholine, **2b**, piperidine and **2c**, pyrrolidine) in acetonitrile at 20°C [27, 29] can be described by the linear free

energy relationship  $\log k = s_N(N+ E)$ , [45–48] and we determined the  $E$  parameters of these electrophiles **1a-c** which are collected in **Figure 12**. We have now used these parameters  $E$  in order to elucidate the relationship between Mayr's electrophilicities  $E$  [45] and Parr's global electrophilicity index  $w$  values [49, 50]. As will be seen, satisfactory correlations between experimentally electrophilic reactivities  $E$  and other properties of these series of para-substituted nitrobenzofurazans **1a-c** are found and discussed. On the other hand, we discuss how the structure–property relationships can be used to evaluate electrophilicity parameter  $E$  and Hammett constant  $\sigma$  values which are not directly accessible.

### 3.4.2 Correlation between electrophilicity parameter ( $E$ ) and global electrophilicity index ( $w$ )

Based on the data listed in **Table 6**, the plot of electrophilicity parameters  $E$  for these series of benzofurazans **1a-c** against their global electrophilicity index  $w$ , determined in this work, was constructed. As can be seen in **Figure 13**, the relationship between  $E$  and  $w$  values is linear ( $r^2 > 0.9799$ ) and results in the following equation:

$$E = -29.785 + 1.545 w \quad (6)$$

It is interesting to note that the relationships parameters  $E$  versus  $w$  have also been reported by many authors. [51–56] The data in **Table 7** are illustrative in this regard. Interestingly, the plot of Eq. (6) can be used to estimate the unknown electrophilicity parameter  $E$  values of other para-substituted benzofurazans. Using the  $w$  values calculated in the present work by DFT//B3LYP/6-31+ g(d,p), the  $E$  of **1d** (X = morpholine,  $E = -18.01$ ), **1e** (X = piperidine,  $E = -18.52$ ), and **1f** (X = pyrrolidine,  $E = -18.78$ ) have been obtained (The structures of title compounds are given in **Figure 2**). The detailed results are already listed in **Table 6**.

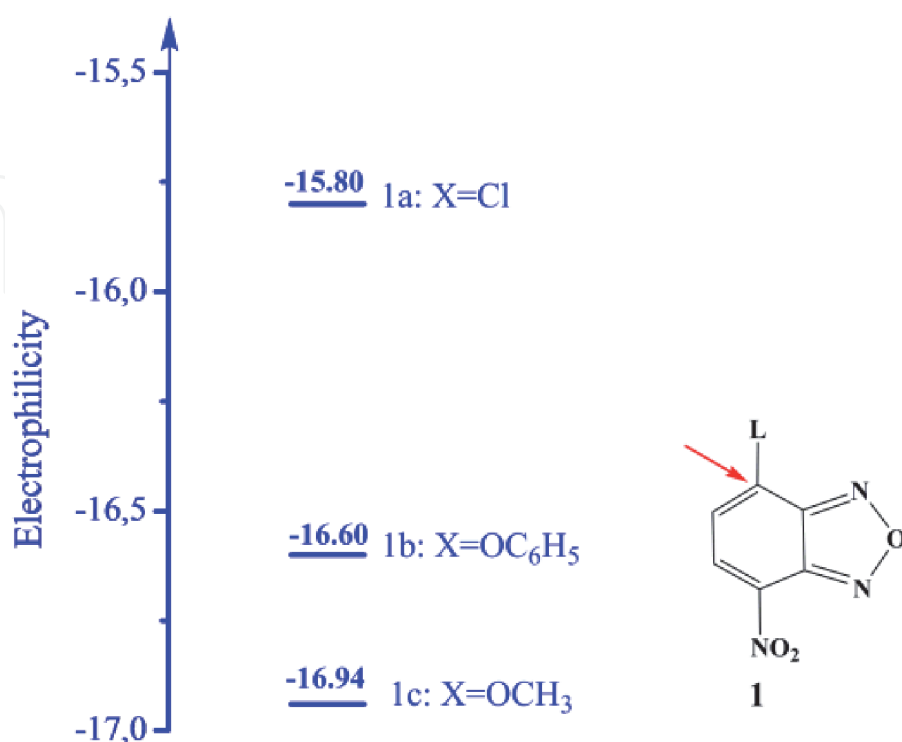


**Figure 12.** Electrophilicity parameters  $E$  of 7- $X$ -4-nitrobenzofurazans **1a-c**. [27, 29].

Benzofurazan	1a	1b	1c	1d	1e	1f
E	-15.80 <sup>a</sup>	-16.60 <sup>b</sup>	-16.94 <sup>a</sup>	-18.01 <sup>c</sup> -16.80 <sup>d</sup>	-18.52 <sup>c</sup> -17.04 <sup>d</sup>	-18.78 <sup>c</sup> -17.20 <sup>d</sup>
w <sup>e</sup>	9.0090	8.6200	8.2670	7.6199	7.2908	7.1228

<sup>a</sup>The E values were taken from Ref. [29].

<sup>b</sup>The E value was taken from Ref. [27].

<sup>c</sup>The E values estimated in this work.

<sup>d</sup>The E values were taken from Ref. [27].

<sup>e</sup>The w values calculated in this work.

**Table 6.**  
 Electrophilicity parameter (E) and global electrophilicity index (w).

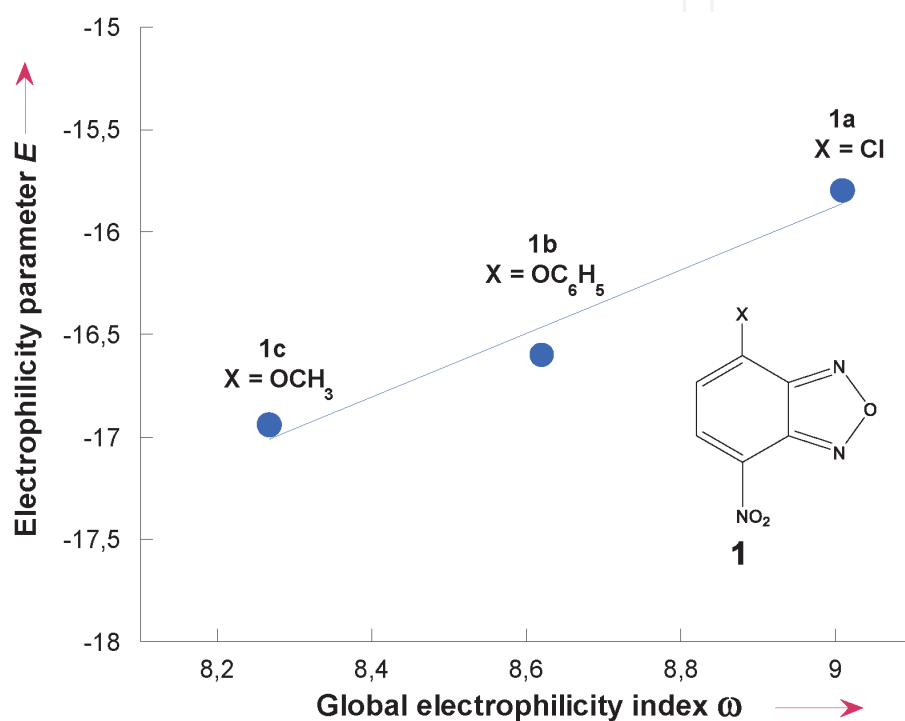
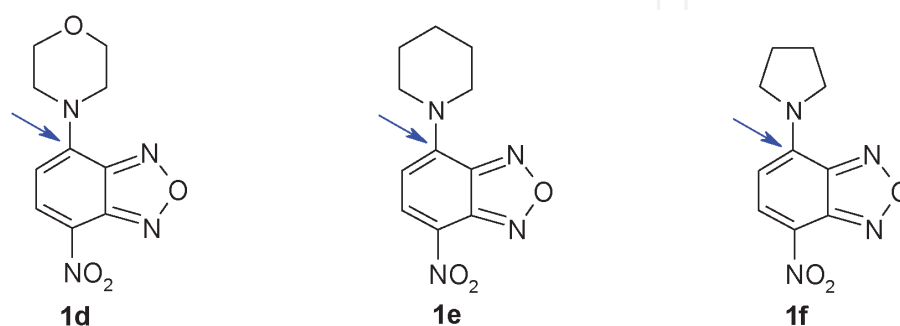


**Figure 13.**  
 Correlation between experimentally determined electrophilicities (E) and global electrophilicity index (w) calculated at DFT//B3LYP/6-31+g(d,p) in acetonitrile for the benzofurazans 1a-c.

Electrophile	Eq.	Ref.	Electrophile	Eq.	Ref.
	$E = -0.24 + 0.153 w$	[51]		$E = -39.26 + 3.36 w$	[54]
	$E = 1.47 + 0.025 w$	[52]		$E = -27.71 + 6.18 w$	[55]
	$E = -12.30 + 0.45 w$ $E = -25.60 + 1.56 w$	[53]		$E = -34.73 + 10.37 w$	[56]

**Table 7.**  
 Correlations of the electrophilicity parameters E of some representative electrophiles with their global electrophilicity w values.

It should be noted that these predicted values of electrophilicity parameters  $E$  are smaller by 1.5 units than those reported values by Raissi and co-workers. [27] In all cases, the agreement between the  $E$  values of benzofurazans **1d-f** estimated using DFT//B3LYP/6-31+g(d,p) and previously reported with the same method of calculation, but recorded in water medium [27] is remarkably good. [57–61]. It is noteworthy to mention that the observed deviations between results give lower accuracy owing to their dependence on solvent polarity and to the added diffuse basis functions, that have also been observed in numerous systems. Chamorro and co-workers, have also observed a satisfactory correlations between the electrophilicity parameter  $E$  of various benzhydrylium cations and their global electrophilicity index  $\omega$  calculated at B3LYP/6-31g(d) and HF/6-31g(d) levels of theory Model I ( $E = -41.60 + 3.57 \omega$ ), Model II ( $E = -40.42 + 2.08 \omega$ ), Model III ( $E = -38.66 + 2.44 \omega$ ) and Model IV ( $E = -47.2 + 20.0 \omega$ ). [62]



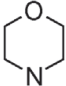
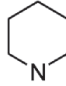
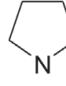
### 3.5 Effect of substituents X on electrophilicity: $E$ vs. $\sigma$ and $w$ vs. $\sigma$ correlations

Examination of the data in **Tables 6** and **8** show that the electrophilicity parameter ( $E$ ) or global electrophilicity index ( $w$ ) of benzofurazans **1a-c** appears to be significantly dependent on the electronic nature of the substituents X, i.e. the  $E$  or  $w$  decrease regularly from X = Cl to X = OCH<sub>3</sub> leading to a nice Hammett-type plots [63, 64] (**Figure 14**), which are defined by the following Equations

$$E = -16.475 + 2.878 \sigma \quad (r^2 = 0.9984) \quad (7)$$

$$w = 8.614 + 1.810 \sigma \quad (r^2 = 0.9897) \quad (8)$$

Correlations between  $E$  and  $\sigma$  parameters or  $E$  and  $w$  of various system have also been reported by many authors. [65–72] Zenz and Mayr, have established that the  $E$  parameters for a series of trans- $\beta$ -nitrostyrenes correlate well with  $\sigma_p$  values of their substituents ( $E = -13.95 + 2.08 \sigma_p$  ( $r^2 = 0.9847$ )). [69] Recently, Rammah and

Substituted	Cl	OC <sub>6</sub> H <sub>5</sub>	OCH <sub>3</sub>			
$\sigma$	0.23 <sup>a</sup>	-0.03 <sup>a</sup>	-0.17 <sup>a</sup>	-0.52 <sup>b</sup> -0.54 <sup>c</sup>	-0.70 <sup>b</sup> -0.72 <sup>c</sup>	-0.79 <sup>b</sup> -0.81 <sup>c</sup>
$\mu^d$	7.23	10.29	9.26	13.57	16.84	17.08

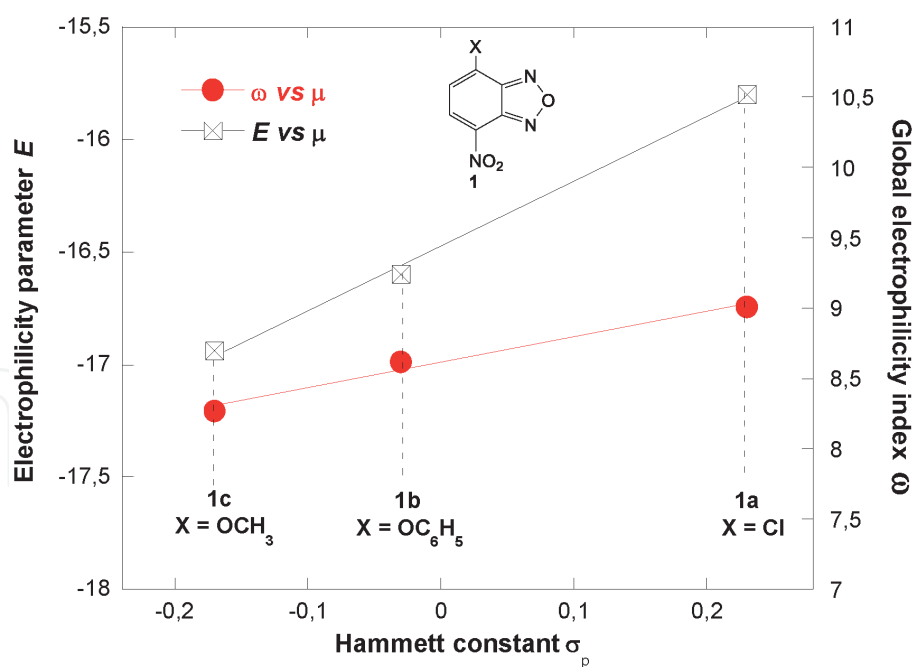
<sup>a</sup>The  $\sigma$  values were taken from Ref. [63, 64].

<sup>b</sup>The  $\sigma$  values calculated by using Eq. (7) with  $E$  from **Table 6**.

<sup>c</sup>Calculated by using Eq. (8) with  $w$  from **Table 6**.

<sup>d</sup>The dipole moment  $\mu$  values calculated in this work.

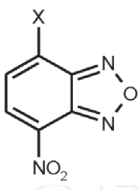
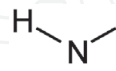
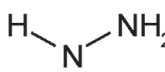
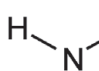
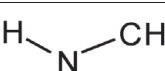
**Table 8.**  
Hammett constants ( $\sigma$ ) values and dipole moment ( $\mu$ , D) values.



**Figure 14.** Correlations of the electrophilicity parameter  $E$  and global electrophilicity index  $w$  versus the Hammett's substituted  $\sigma_p$  values. The values of  $E$  and  $w$  are given in **Table 6**. The  $\sigma_p$  values were taken from Ref. [63, 64].

co-workers, have also observed a linear correlation between the electrophilicity parameters  $E$  of a series of 2-N-(4'-X-phenyl)-4,6-dinitrobenzotriazole 1-oxides and the Hammett's substituent constants  $\sigma$  ( $E = -11.15 + 2.28 \sigma$  ( $r^2 = 0.9878$ )). [65]

In order to test the applicability of Eq. (7) for the prediction of the Hammett's constants  $\sigma_p$  of other groups, we have calculated the global electrophilicity index ( $w$ ) of benzofurazans **1 g-j** (**1 g**: X = HNOH, **1 h**: X = HNNH<sub>2</sub>, **1 i**: X = HNH and **1 j**: X = HNCH<sub>3</sub>). The results are listed in **Table 9** which also includes the  $\sigma_p$  values

	Substituent X	$w^a$	$\mu^b$	$\sigma_p^{Cal, c}$	$\sigma_p^{Exp, d}$
<b>1 g</b>		7.893	12.88	-0.34	-0.34
<b>1 h</b>		7.630	12.26	-0.53	-0.55
<b>1 i</b>		7.501	13.69	-0.60	-0.66
<b>1 j</b>		7.356	15.30	-0.68	-0.70

<sup>a</sup>The  $w$  values calculated in this work.  
<sup>b</sup>The dipole moment  $\mu$  values calculated in this work.  
<sup>c</sup>The  $\sigma_p^{Cal}$  values calculated by using Eq. (8) with  $w$  from **Table 5**.  
<sup>d</sup>The  $\sigma_p^{Exp}$  values were taken from Ref. [63, 64].

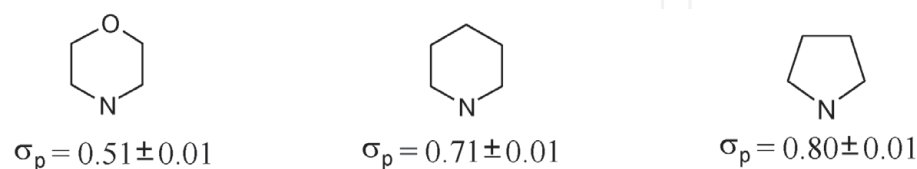
**Table 9.** Comparison between calculated and experimental reported Hammett's constants  $\sigma_p$  for the HNOH, HNNH<sub>2</sub>, HNH and HNCH<sub>3</sub> groups.



previously published. [63, 64] As well be seen, **Table 2** clearly shows that the calculated  $\sigma_p$  values are in good agreement with the experimental data.

Most importantly, the satisfactory correlations shown in **Figure 14** can be employed to obtain more information about the unknown Hammett's substituent constants ( $\sigma$ ) of morpholine, piperidine and pyrrolidine groups.

Substitution of the  $E$  and  $w$  values for benzofurazans **1d-f** into the correlation Eqs. (7) and (8), the Hammett's  $\sigma_p$  values are thus obtained for the three leaving-groups. As can be seen in **Table 8**, the  $\sigma_p$  values estimated in the present work using work using Eqs. (7) or (8) are similar but relatively large compared with those previously reported ( $-0.47 < \sigma_p < -0.24$ ). [27] The major reason for the overestimation can, at least in part, be understood in terms of solvent polarity and also the used on the basis set with diffuse functions.



### 3.6 Correlation between dipole moment ( $\mu$ ) and Hammett's substituent constants ( $\sigma$ )

As shown in **Table 8** and **Figure 15**, the dipole moments ( $\mu$ ) calculated at DFT//B3LYP/6-31+g(d,p) for these series of benzofurazans **1a-f** are highly sensitive to the electronic nature of the substituent X, e.g., it decreases from  $\mu = 17.08$  D to  $\mu = 7.23$  D as the substituent X changes from a strong electron-withdrawing group (X = Cl) to a strong electron-donating group (X = morpholine). The linear relationship as expressed by Eq. (9) relates the dipole moment  $\mu$  for **1a-f** directly to the Hammett's substituent constant  $\sigma$ .

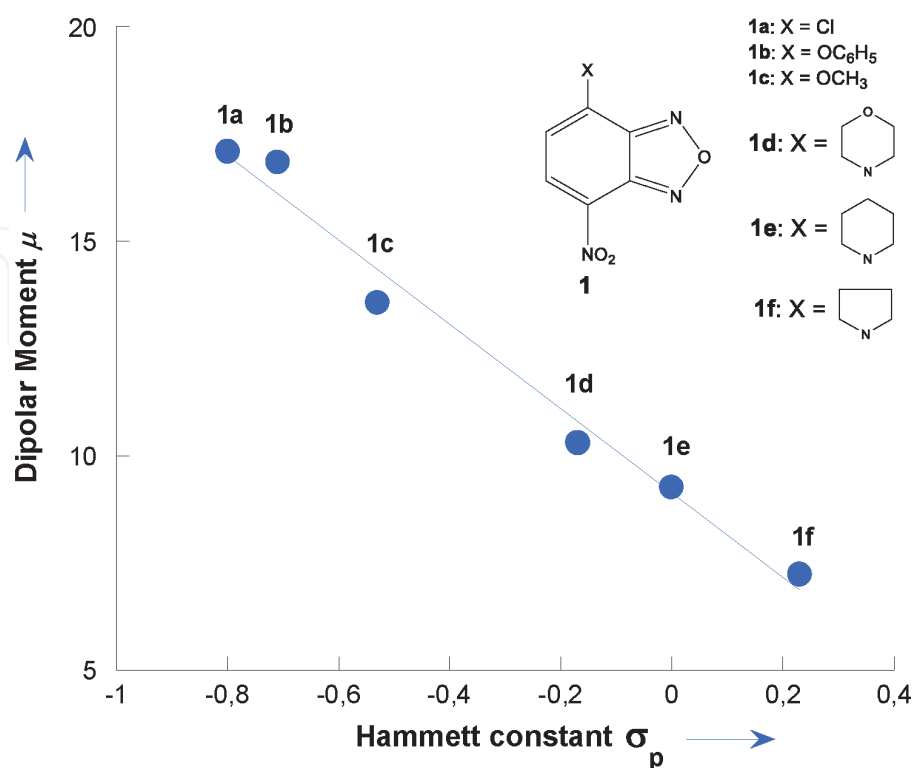


**Figure 15.** Correlation between calculated dipole moment ( $\mu$ ) for the benzofurazans **1a-f** and Hammett's substituent constant  $\sigma$  calculated at DFT//B3LYP/6-31+g(d,p) in acetonitrile.

$$\mu = 9.135 - 9.839 \sigma \quad (r^2 = 0.9908) \quad (9)$$

On the other hand, comparing the electrophilicity parameter  $E$  and global electrophilicity index  $w$  with the dipole moment ( $\mu$ ), we found that the  $E$  and values  $w$  correlate well with the  $\mu$  as shown in **Figure 16**. In addition, the high dipole moment values being related to the strong effect exerted by the electron-donating group X clearly indicate that our benzofurazans **1b-j** can offer certain potential for nonlinear optical (NLO) applications.

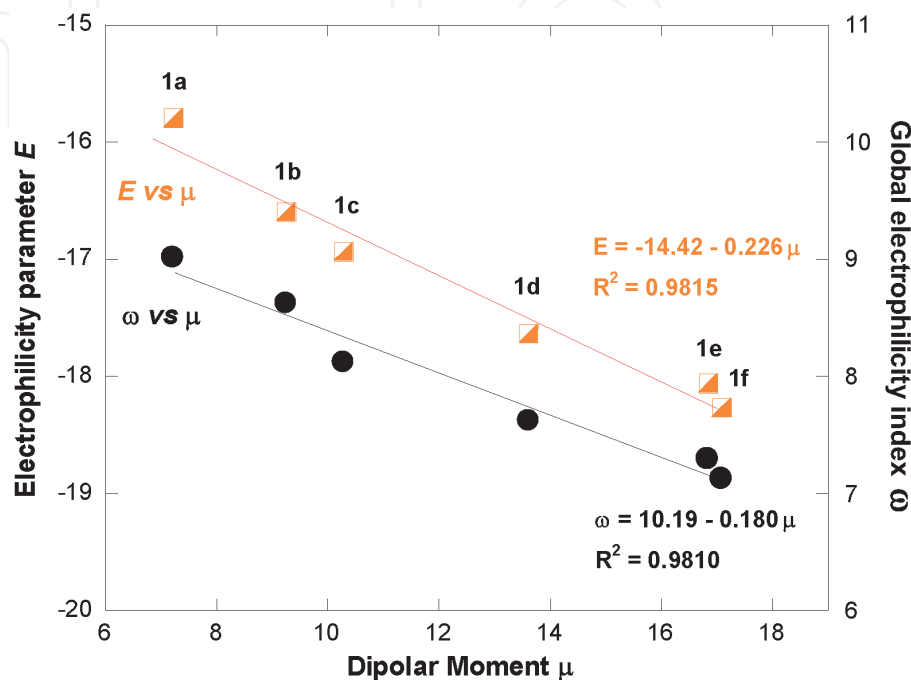


**Figure 16.** Correlation  $E$  vs.  $\mu$  and  $w$  vs.  $\mu$  for the benzofurazans **1a-f** calculated at DFT//B3LYP/6-31+g(d,p) in acetonitrile.

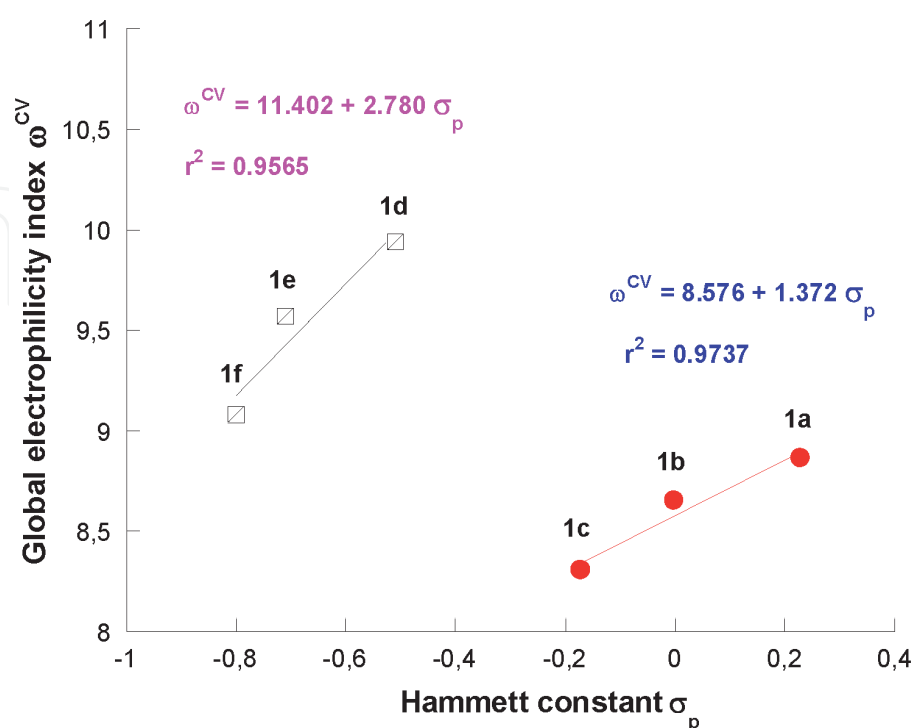


**Figure 17.** Correlations of the global electrophilicity index  $w^{CV}$  of the benzofurazans **1a-f** versus the Hammett's substituted  $\sigma_p$  values. The values of  $w^{CV}$  are given in **Table 1**. The  $\sigma_p$  values were taken from Ref. [63, 64].

### 3.7 Correlation between global electrophilicity index $w^{CV}$ and Hammett's substituent constants ( $\sigma_p$ )

To further extend the generality of the structure–property relationships to the global electrophilicity index  $w^{CV}$  calculated from the Cyclic Voltammetry (CV) listed in **Table 1**, we examined correlations  $w^{CV}$  vs.  $\sigma_p$ ,  $w^{CV}$  vs.  $E$  and  $w^{CV}$  vs.  $w$ . As

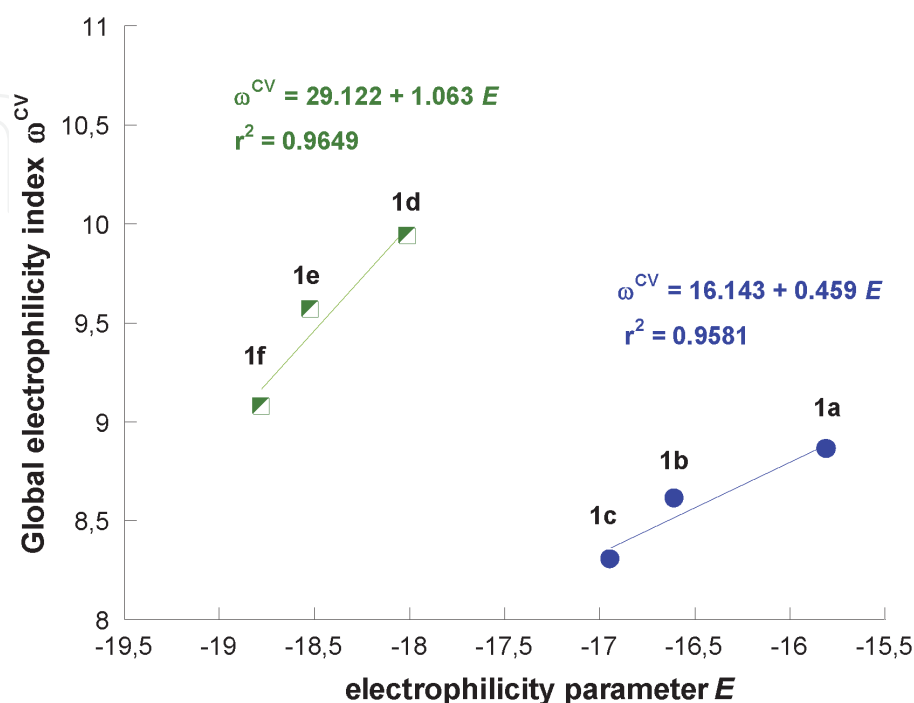


**Figure 18.**

Correlations between global electrophilicity index  $w^{CV}$  and experimentally determined electrophilicities  $E$  for the benzofurazans **1a-c**. the values of  $w^{CV}$  are given in **Table 1** and values of  $E$  are given in **Table 6**.

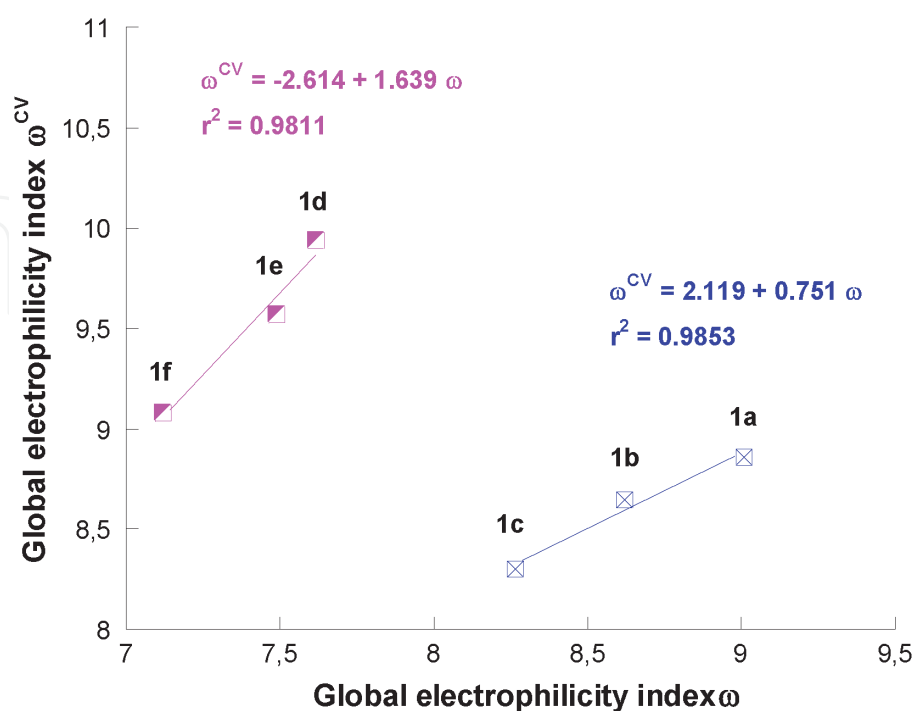


**Figure 19.**

Correlations of the global electrophilicity index  $w^{CV}$  and global electrophilicity index  $w$  calculated at DFT//B3LYP/6-31 + g(d,p) in acetonitrile for the benzofurazans **1a-f**. the values of  $w^{CV}$  are given in **Table 1** and values of  $w$  are given in **Table 6**.

can be seen, the plotting of the  $w^{CV}$  values determined above (see **Table 1**) versus the known Hammett's constant  $\sigma_p$  values of substituent X gives rise to two separate linear correlations corresponding to a different behavior of Cl, OCH<sub>3</sub>, OC<sub>6</sub>H<sub>5</sub> groups and morpholinyl, piperidinyl and pyrrolidinyl groups (**Figure 17**).

Similar behaviors have also been obtained when the global electrophilicity index  $w^{CV}$  values were plotted against the electrophilicity parameter  $E$  or the global electrophilicity index  $w$  (**Figures 18 and 19**). The reason for this apparent disparity is not clear at this stage. Clearly, more investigate is necessary to explicate this behavior.

#### 4. Conclusion

The reaction between NBD-Cl and morpholine, piperidine or pyrrolidine, as nucleophile group, proceeds normally by a S<sub>N</sub>Ar attack affording 4,7-di-substituted benzofurazans. They were thoroughly analyzed electrochemically and optically by means of Cyclic Voltammetry (CV) and UV-Vis and time resolved photoluminescence (TR-PL), respectively.

Complementary study based on density function theory (DFT) and its extent TD-DFT were also conducted to unravel the electronic structure, the simulated optical spectra and to further understand the structure property relationships of the investigated compounds. The used procedure based theoretical calculations allows deducing the electronic parameters related to the HOMO and LUMO energy levels and their energy differences. These levels are accessible by measuring the peak potentials of the oxidation and reduction reactions. It is found that the measured energy levels are in close agreement with the values computed from DFT method. Specific nucleophile-electrophile interactions in S<sub>N</sub>Ar reactions were expected to be governed by three main types of non-covalent bonds (O—H, N—O and N—H). Importantly, the compounds absorb visible light at longer wavelengths. In addition, the S<sub>N</sub>Ar attack leads to intra-molecular charge transfer of formed compounds and thus provides a remarkably slow non-radiative decay from the excited state. Investigation of photo-physical properties revealed importance of intra-molecular twisting on excited (S<sub>1</sub>) states.

As verified by experimental and calculated results, the obtained molecules, by S<sub>N</sub>Ar reactions, were modulated by intra-molecular non-covalent interactions that force the co-planarity and the rigidity of the structures yielding an efficient intra-molecular charge transfer (ICT). Thus, the nucleophile substituents acting as electron-donating groups in S<sub>N</sub>Ar reaction afford to obtain materials with interesting nonlinear optical (NLO) response. In addition, the photo-optical data corroborated with TD-DFT approach were discussed in correlation with the structural architecture of each compound. We have shown the high efficiency fluorescent NBD-Morph compound that emits green to orange color at wavelength maximum of 559-603 nm.

The theoretical optimized parameters have been found to be in good agreement with the corresponding experimental data and results in the literature. Satisfactory linear correlation has been demonstrated between the parameters  $E$  and the global electrophilicity index  $w$  for the electrophilic reactivity at the C-X position of nitrobenzofurazans **1a-d**. Accordingly, structure-property relationships were found to be able to evaluate the unknown electrophilicity parameter  $E$  of 7-X-4-nitrobenzofurazans **1d-f**. Alternatively, the validity of Eqs. (7) and (8) has been satisfactorily verified by comparison of calculated and previously reported, in the literature, of the Hammett constant  $\sigma_p$  values of HNOH, HNNH<sub>2</sub>, HNH and HNCH<sub>3</sub> groups.

## **Conflict of interest**

The authors declare no conflict of interest.

IntechOpen

## **Author details**

Hanen Raissi<sup>1</sup>, Imen Chérif<sup>2</sup>, Hajer Ayachi<sup>1</sup>, Ayoub Haj Said<sup>3,4</sup>, Fredj Hassen<sup>5</sup>, Sahbi Ayachi<sup>2\*</sup> and Taoufik Boubaker<sup>1\*</sup>

1 Laboratoire de Chimie Hétérocyclique, Produits Naturels et Réactivité (LR11ES39), Faculté des Sciences, Université de Monastir, Monastir, Tunisia

2 Laboratory of Physico-Chemistry of Materials (LR01ES19), Faculty of Sciences, University of Monastir, Tunisia


3 Laboratoire Interfaces et Matériaux Avancés (LIMA), Faculté des Sciences, Université de Monastir, Monastir, Tunisia

4 Centre de Recherche en Microélectronique et Nanotechnologie, Technopôle de Sousse, Sousse, Tunisia

5 Laboratoire de Micro-Optoélectronique et Nanostructures (LR99/ES29), Faculté des Sciences, Université de Monastir, Monastir, Tunisia

\*Address all correspondence to: ayachi\_sahbi@yahoo.fr and boubaker\_taoufik@yahoo.fr

## **IntechOpen**

© 2021 The Author(s). Licensee IntechOpen. This chapter is distributed under the terms of the Creative Commons Attribution License (<http://creativecommons.org/licenses/by/3.0>), which permits unrestricted use, distribution, and reproduction in any medium, provided the original work is properly cited. 



## References

- [1] F. Qian, C. Zhang, Y. Zhang, W. He, X. Gao, P. Hu, Z. Guo, *J. Am. Chem. Soc.* 131 (2009) 1460-1468.
- [2] T. Yamaguchi, M. Asanuma, S. Nakanishi, Y. Saito, M. Okazaki, K. Dodo, M. Sodeoka, *Chem. Sci.* 5 (2014) 1021-1029.
- [3] P. B. Ghosh, M.W.Whitehouse. *Biochem. J.* 108 (1968) 155-156.
- [4] P. B. Ghosh, M.W.Whitehouse. *J. Med. Chem.* 11(1968) 305-311.
- [5] D. Castagnolo, M. Pagano, M. Bernardini, M. Botta, *Tetrahed. Lett.* 53 (2012) 5008-5011.
- [6] C. Toriumi and K. Imai, *Anal. Chem.*, 74 (2002) 2321-2327.
- [7] T. Kajiro, Y. Nakajima, T. Fukushima and K. Imai, *Anal. Chem.*, 74 (2002) 4519-4525.
- [8] H.C. Ting, Y.T. Yang, C.H. Chen, J.H. Lee, J. H. Chang, C.I. Wu, T. L. Chiu, C. F. Lin, C. L. Chung, K. T. Wong, *ChemSusChem* 9 (2016) 1433-1441.
- [9] J. Mori, T. Kaino, *Phys. Lett. A* 127 (1988) 259.
- [10] L. Johnson, S. Lagerkvist, P. Lindroth, M. Ahnoff, K. Martinsson, *Anal. Chem.*, 54 (1982) 939-942.
- [11] D. Dal Monte, E. Sandri, L. Di Nunno, S. Florio, P. Todesco, *Chimica e Industria*, 53 (1971) 940-942.
- [12] R.A. Manderville and E. Buncel, *J. Chem. Soc. Perk. T. 2*, (1993)1887-1894.
- [13] S. Uchiyama, T. Santa, T. Fukushima, H. Homma, K. Imai, *J. Chem. Soc. Perk. T. 2*, (1998) 2165-2173.
- [14] M. Bem, M. T. Caproiu, D. Stoicescu, T. Constantinescu, and A. T. Balaban, *Cent. Eur. J. Chem.*, 2003, 1, 260.
- [15] I. Jamaoui, T. Boubaker, R. Goumont, *Int. J. Chem. Kinet.* 45 (2013) 152-160.
- [16] W.J. Wang, J.M. Xia, X. Hai, M.L. Chen, J.H. Wang, *Environ. Sci. Nano*, 4 (2017) 1037-1044.
- [17] R. Poulain, D. Horvath, B. Bonnet, C. Eckhoff, B. Chapelain, M.-C. Bodinier, and B. Deprez, *J. Med. Chem.*, 44 (2001) 3378.
- [18] N. Lavignac, C. J. Allender, and K. R. Brain, *Tetrahedron Lett.*, 45 (2004) 3625.
- [19] M. Bem, M. Vasilescu, M. T. Caproiu, C. Draghici, A. Beteringhe, T. Constantinescu, M. D. Banciu, and A. T. Balaban, *Cent. Eur. J. Chem.*, 2 (2004) 672-685.
- [20] Jun-ichi Aihara, Reduced HOMO-LUMO Gap as an Index of Kinetic Stability for Polycyclic Aromatic Hydrocarbons, *J. Phys. Chem. A* 103, 37 (1999) 7487-7495.
- [21] Jun-ichi Aihara, *Phys. Chem. Chem. Phys.*, 2000, 2, 3121-3125.
- [22] R. Zaier, S. Ayachi, *Optik*, 239 (2021) 166787.
- [23] R. Zaier, S. Hajaji, M. Kozaki, S. Ayachi, *Opt. Mat.* 91C (2019) 108-114.
- [24] A. J. Boulton, A. R. Katrizky, A. M. Hamid, *J. Chem. Soc.*, 1967 (2005) 2007.
- [25] J. C. Hallé, M. Mokhtari, P. Soulié, M. J. Pouet, *Can. J. Chem* 75 (1997) 1240.
- [26] M. R. Crampton, L. M. Pearce, L. C. Rabbitt, *J. Chem. Soc., Perkin trans 2* (2002) 257.

- [27] H. Raissi, H. Ayachi, F. Mahdhaoui, S. Ayachi, T. Boubaker, *J. Mol. Str.* 1224 (2021) 128843.
- [28] H. Ayachi, H. Raissi, F. Mahdhaoui, T. Boubaker, *Int. J. Chem. Kinet.* 52 (2020) 655-668.
- [29] H. Raissi, I. Jamaoui, R. Goumont, T. Boubaker, *Int. J. Chem. Kinet.* 49 (2017) 835-846.
- [30] F. Mahdhaoui, R. Zaier, N. Dhahri, S. Ayachi, T. Boubaker, *Int. J. Chem. Kinet.* 51 (2019) 249-257.
- [31] I. Messaoudi, I. Aribi, Z. Zouhour S. Ayachi, M. Othman, A.H. Said, *J. Mol. Str.* 1231 (2021) 129810.
- [32] A. Abbotto, L. Beverina, N. *manfredi*, G. A. Pagani, G. Archetti, H. G. Kuball, C. Wittenburg, J. heck, J. Holtman, *Chem. Eur. J.* 15 (2009) 6175-6185.
- [33] J. A. Davies, A. Elangovan, P. A. Sullivan, B. C. Olbricht, D. H. Bale, T.R. Ewy, C.M. Isborn, B.E. Eichinger, B.H. Robinson, P.J. Reid, X. Li, L. R. Dalton, *J. Am. Chem. Soc.* 130 (2008) 10565-10575.
- [34] Z. Zaaboub, F. Hassen, H. Maaref, *Sol. Stat. Comm.* 314-315 (2020) 113913.
- [35] A. D. Becke, *J. Chem. Phys.* 98 (1993) 5648-5652.
- [36] C. Lee, W. Yang, R. G. Parr, *Phys. Rev.* 37 (1988), 785-789.
- [37] M. J. Frisch., et al. Gaussian 09, Revision A.01, Gaussian: Wallingford, CT (2009).
- [38] Dennington, R.D., Keith, T.A. and Millam, J.M. (2008) GaussView 5.0.8, Gaussian.
- [39] J. L. Bredas, R. Silbey, D. S. Boudreaux, and R. R. Chance, *J. Am. Chem. Soc.* 105 (22) (1983) 6555-6559.
- [40] Heberer, H.; Matschiner, H., *J. Prakt. Chem.*, 328 (1986) 261-274.
- [41] S. Ayachi, S. Ghomrasni, M. Bouachrine, M. Hamidi, K. Alimi, *J. Mol. Str.* 1036, (2013) 7-18.
- [42] S. Ayachi, S. Ghomrasni, K. Alimi, *J. App. Polym.Sci.* 123 (2012) 2684-2696.
- [43] R. G. Parr, L. V. Szentpaly, S. Liu, *J Am Chem Soc.* 1999, 121, 1922-1924.
- [44] Parr, R. G, Yang, W. *Density Functional Theory of Atoms and Molecules*; Oxford University Press: New York 1989.
- [45] H. Mayr, M. Patz, *Angew. Chem. Int. Ed. Engl.* 33 (1994) 938-957.(b) H. Mayr, B. Kempf, A. R. Ofial, *Acc. Chem. Res.* 36 (2003) 66-77.
- [46] S. Ben Salah, F. Necibi, R. Goumont, T. Boubaker. *ChemistrySelect.* 5 (2020) 7648-7657.
- [47] S. Souissi, W. Gabsi, A. Echaieb, J. C. Hierso, P. Fleurat-Lessard, T. Boubaker. *RSC Advances.* 10 (2020) 28635-28643.
- [48] Z. Li, R. J. Mayer, A. R. Ofial, and H. Mayr. *J Am Chem Soc.* 142 (2020) 18, 8383-8402.
- [49] R. G. Parr, R. G. Pearson, *J. Am. Chem. Soc.* 105 (1983) 7512-7516.
- [50] R. G. Parr, L. V. Szentpaly, S. Liu. *J. Am. Chem. Soc.* 121 (1999) 1922-1924.
- [51] D. S. Allgäuer, H. Jangra, H. Asahara, Z. Li, Q. Chen, H. Zipse, A. R. Ofial, H. Mayr. *J. Am. Chem. Soc.*, 139 (2017) 13318-13329.
- [52] Z. Li, H. Jangra, Q. Chen, P. Mayer, A. R. Ofial, H. Zipse, H. Mayr. *J. Am. Chem. Soc.* 140 (2018) 5500-5515.
- [53] W. Gabsi, T. Boubaker, R. Goumont. *Int. J. Chem. Kinet.* 48 (2016) 266-273.

- [54] P. Pérez, A. Labbé. *J. Org. Chem.* 67 (2002) 4747-4752.
- [55] L. R. Domingo, P. Pérez, R. Contreras. L. R. Domingo, P. Pérez, R. Contreras. *Tetrahed.* 60 (2004) 6585-6591.
- [56] D. S. Allgäuer, H. Jangra, H. Asahara, Z. Li, Q. Chen, H. Zipse, A. R. Ofial, H. Mayr. *J. Am. Chem. Soc.* 139 (2017) 13318-13329.
- [57] Q. Chen, P. Mayer, H. Mayr. *Angew Chem Int Ed* 55 (2016) 12644-12667.
- [58] R. J. Mayer, P. W. A. Allihn, N. Hampel, P. Mayer, S. A. Sieber, A. R. Ofia. *Chem. Sci.* 12 (2021) 4850-4865.
- [59] S. Ben Salah, T. Boubaker, R. Goumont. *Int J Chem Kinet* 49 (2017) 576-583.
- [60] E. Follet, P. Mayer, H. Mayr, *Eur J Org Chem.* 2016, 4050-4058.
- [61] N. Dhahri, T. Boubaker, R. Goumont. *J Phys Org Chem.* , 27 (2014) 484.
- [62] E. Chamorro, M. Duque-Noreña, P. Pérez. *J Mol Struct.* 896 (2009) 73-79.
- [63] C. Hansch, A. Leo, R. W. Taft. *Chem. Rev.* 91 (1991) 185-195.
- [64] Hammett L. P. *Reaction Rates, Equilibria and Mechanism.* Mc Graw-Hill, New York, 2nd edn, 1970.
- [65] M. Rammah, F. Mahdhaoui, W. Gabssi, T. Boubaker. *ChemistrySelect.* 6 (2021) 4424-4431.
- [66] O. Kaumanns, H. Mayr. *J Org Chem.* 73 (2008) 2738-2745.
- [67] H. Asahara, H. Mayr. *Chem Asian J.* 7 (2012) 1401, 1407.
- [68] K. Azaiez, N. Dhahri, T. Boubaker. *Int J Chem Kinet.* 49 (2017) 847-858.
- [69] I. Zenz, H. Mayr. *J Org Chem.* 76 (2011) 9370-937.
- [70] J. Ammer, C. Nolte, H. Mayr. *J Am Chem Soc.* 134 (2012) 13902-13911.
- [71] K. Troshin, C. Schindele, H. Mayr. *J Org Chem.* 76 (2011) 9391-9408.
- [72] D. Richter, N. Hampel, T. Singer, A. R. Ofial, H. Mayr. *Eur J Org Chem.* 2009, 3203-3211.